water

MDPI

*Article*

# Research on Temperature Control Index for High Concrete Dams Based on Information Entropy and Cloud Model from the View of Spatial Field

**Guang Yang [1,†], Jin Sun [2,*,†], Jianwei Zhang [1], Jingtai Niu [3,*], Bowen Luan [1], Zhendong Huang [1] and Ahui Zhao [1]**

[1] School of Water Conservancy, North China University of Water Resources and Electric Power, Zhengzhou 450045, China; yangguang2019@ncwu.edu.cn (G.Y.); zhangjianwei@ncwu.edu.cn (J.Z.); bowenluan@outlook.com (B.L.); hhzd493@outlook.com (Z.H.); zhaoahui1998@outlook.com (A.Z.)
[2] College of Surveying and Geo-Informatics, North China University of Water Resources and Electric Power, Zhengzhou 450045, China
[3] School of Hydraulic and Ecological Engineering, Nanchang Institute of Technology, Nanchang 330099, China
* Correspondence: sunjin@ncwu.edu.cn (J.S.); niujingtai@163.com (J.N.)
† These authors contributed equally to this work.

**Abstract:** It is significant to adopt scientific temperature control criteria for high concrete dams in the construction period according to practical experience and theoretical calculation. This work synthetically uses information entropy and a cloud model and develops novel in situ observation data-based temperature control indexes from the view of a spatial field. The order degree and the disorder degree of observation values are defined according to the probability principle. Information entropy and weight parameters are combined to describe the distribution characteristics of the temperature field. Weight parameters are optimized via projection pursuit analysis (PPA), and then temperature field entropy (TFE) is constructed. Based on the above work, multi-level temperature control indexes are set up via a cloud model. Finally, a case study is conducted to verify the performance of the proposed method. According to the calculation results, the change law of TFEs agrees with actual situations, indicating that the established TFE is reasonable, the application conditions of the cloud model are wider than those of the typical small probability method, and the determined temperature control indexes improve the safety management level of high concrete dams. Research results offer scientific reference and technical support for temperature control standards adopted at other similar projects.

**Keywords:** high concrete dam; in situ observation data; temperature field; temperature control index; information entropy; cloud model; dam safety

check for updates

**Citation:** Yang, G.; Sun, J.; Zhang, J.; Niu, J.; Luan, B.; Huang, Z.; Zhao, A. Research on Temperature Control Index for High Concrete Dams Based on Information Entropy and Cloud Model from the View of Spatial Field. *Water* **2023**, *15*, 4023. https://doi.org/10.3390/w15224023

Academic Editor: Giuseppe Oliveto

Received: 7 September 2023
Revised: 3 November 2023
Accepted: 14 November 2023
Published: 20 November 2023

**Copyright:** © 2023 by the authors. Licensee MDPI, Basel, Switzerland. This article is an open access article distributed under the terms and conditions of the Creative Commons Attribution (CC BY) license (https://creativecommons.org/licenses/by/4.0/).

## 1. Introduction

Several high concrete dams have been constructed in China over the years, e.g., the Xiluodu arch dam (285.50 m) and the Xiangjiaba gravity dam (162.00 m), as shown in Figure 1a,b [1–8]. These huge projects have tremendously contributed to the economic growth and social development of China. However, they also pose serious security risks, which could cause unpredictable and disastrous consequences. Historically, severe concrete dam failure accidents occurred and caused vast economic losses and causalities, such as the St. Francis dam, the Malpasset dam, and the Vajont dam [9–11]. Therefore, governments of the world set strict requirements on the safe construction and operation of concrete dams [12], especially for high concrete dams. Instead of a sudden occurrence, a dam accident is a gradual process from quantitative to qualitative changes. In situ observation and risk assessment are essential for making informed decisions about the construction safety of high concrete dams, with the ultimate goal of protecting both people and property [13]. If robust and reliable real-time safety monitoring strategies are conducted, then most hidden dangers can be found and catastrophic accidents can be avoided [14–16].

(**a**) (**b**)

**Figure 1.** Typical high concrete dams: (**a**) Xiluodu arch dam and (**b**) Xiangjiaba gravity dam.

Concrete temperature is an important in situ observation indicator for concrete dams [17–19]. Several factors, e.g., cement hydration heat, atmospheric temperature, water temperature, etc., play an important role in concrete temperature variation. Concrete materials have poor temperature conductivity. The influence of temperature is mainly reflected in temperature stress. If temperature stress exceeds the threshold, then it can cause dam cracks. Adopting scientific temperature control methods [20–22] can effectively prevent dam cracks, which is crucial to guarantee dam safety. Conventionally, researchers focus on investigating single-point control indexes. However, with the continuous construction of ultra-high concrete dams, single-point indexes cannot meet practical demands. There is an urgent need to construct temperature control indexes from the perspective of the spatial field. Chen et al. proposed a temperature control approach by using the finite element (FE) method, and on this basis, the temperature field evaluation and the thermal-induced stress of the discussed roller-compacted-concrete (RCC) dam were analyzed [23]. Chen et al. used the AdaBoost-ANN algorithm to reconstruct the temperature field of concrete arch dams. The calculation results showed that the proposed algorithm is convenient for dam safety assessment [24]. Pan et al. used the convolutional neural network to analyze the temperature field distribution of the Xiaowan dam, and this method can accurately predict possible thermal cracks on the dam surface [25]. Hou et al. used the FE method to invert the thermal parameters of dam concrete. The calculation results efficiently reflect the temperature field distribution of the discussed ultra-high arch dam [4]. Zhou et al. applied the distributed temperature sensing technology to monitor the temperature field distribution of high-arch dams under construction [26]. In China, cold areas play an important role in further hydropower development. Compared with regions with a mild climate, cold areas where cold waves appear frequently have a large day-night temperature difference, a low annual average temperature, etc., and many scientific problems need to be solved urgently. Although there has been some progress in research related to the spatial temperature field, in-depth research remains rare, especially for those using in situ observation data.

Information entropy, also known as Shannon entropy, is a measure of uncertainty degree caused by insufficient or chaotic information in a system. The greater the information entropy, the higher the chaotic degree and uncertainty degree the studied system shows. Many applications have been employed in the field of dam safety monitoring. Chen et al. used information entropy theory to analyze the seepage characteristics of complex rock mass dams [27]. Su et al. comprehensively applied information entropy theory and the FE method to analyze the stress and deformation of concrete-faced rockfill dams [28]. Cui et al. proposed the multi-time-scale mutual information entropy method to reveal the cyclic synchronous changes of drought-flood abrupt alternation in the Three Gorges reservoir area [29]. Lei et al. employed information entropy to characterize the spatial deformation

distribution of high concrete dams. On this basis, the multi-level early-warning indexes were constructed by applying the typical small probability method [30]. Zheng et al. used Copula entropy and mutual information theory to analyze and process in situ observation data of dams, effectively reducing the influence of correlations among different factors [31]. Huang et al. constructed the viscoelastic control indexes for monitoring the deformation safety of gravity dams in alpine regions by comprehensively using the typical small probability method and the maximum entropy method [32]. Zhang et al. used the maximum entropy method to determine operational control loads of concrete dams according to deformation observation data, and the analysis results showed that the proposed method, compared with traditional approaches, has better performances [33]. Qin et al. used weighted fusion entropy and Hurst exponent difference to evaluate the crack evolution of concrete dams [34]. Information entropy, as an intelligent and information-based mathematical method, not only lays a theoretical foundation for measuring uncertainty in random events, but also possesses broad universality and scalability to describe system state evolution. Further research needs to be conducted to characterize the evolution laws of high concrete dam temperature fields based on information entropy theory and then to construct reasonable control indexes for ensuring dam safety.

The cloud model algorithm is a mathematical model using probability theory to describe and quantify uncertain information. It consists of two parts, i.e., a cloud generator and a cloud transformation. Forward and reverse cloud generators can generate cloud droplets and determine mathematical features, respectively. Cloud transformation converts cloud droplets into a probability distribution used for further analysis. The cloud model possesses strong abilities in handling uncertain and imprecise information, which has been applied in various fields, e.g., data mining, decision-making, and pattern recognition. For dam safety monitoring, the cloud model has also achieved successful applications. Han et al. proposed the cloud model-Monte Carlo coupling model that can accurately evaluate risk degree in dam safety management [35]. Wu et al. integrated the cloud model and Dempster-Shafer evidence theory to assess the safety state of tailing dams. The developed approach has strong robustness and a fault-tolerant capacity [36]. Li et al. used the cloud model to analyze in situ observation data of dams, and the proposed method has good performance in discovering abnormal values [37]. Sang et al. developed the extended cloud model and the extended analytic hierarchy process method to address uncertainty problems in the safety assessment of dams [38]. Guo et al. used a cloud model and modal strain energy to identify uncertain damage problems caused by noise [39]. According to the above analyses, the cloud model algorithm can achieve the conversion of qualitative concepts into quantitative data, which provides an effective way to construct temperature control indexes for the multi-level risk management of high concrete dams.

Consequently, by synthetically using information entropy and a cloud model, this study develops temperature control indexes based on in situ observation data. The paper is organized as follows. In Section 2, temperature field entropy (TFE) for describing the evolution characteristics of temperature fields is established, and projection pursuit analysis (PPA) is explored to optimize weight parameters. Section 3 investigates the principle of the cloud model, and then the cloud model-based temperature control indexes are constructed. Section 4 conducts a case study to verify the proposed method. In Section 5, the main conclusions of the research are summarized, and some suggestions are provided.

## 2. Temperature Field Characterization Using Information Entropy

### 2.1. TFE Construction

The evaluation process of dam temperature can be roughly divided into two stages, i.e., the construction period and the operation period [40–42]. During the construction period, the temperature field of the dam body is affected by multiple factors, such as cement hydration heat, artificial cooling, and ambient temperature. In the stage of operation, cement hydration heat has basically dissipated, and the temperature field is affected by ambient temperature, e.g., air temperature and water temperature [43–46]. Concrete

temperature has a significant impact on the stability of the dam during the construction period, but its effects during regular operation afterward are essentially insignificant. This work mainly focuses on the construction period, and information entropy is used to characterize the temperature field evaluation of high concrete dams.

Here, $\delta_{ij}$ denotes the observation value of the $i$th observation point on the $j$th observation date, the corresponding order degree is recorded as $u_{ij}$, $\omega_i$ denotes the weight parameter of the $i$th point, $i = 1, 2, \cdots, n$ and $n$ is the total number of observation points. Under the condition of temperature increase, $u_{ij}$ is defined as follows:

$$u_{ij} = F_i(\delta_{ij}) = \int_{-\infty}^{\delta_{ij}} f_i(\delta) \mathrm{d}\delta, \tag{1}$$

where $f_i(\delta)$ is the probability density function of $\delta_{ij}$, and $F_i(\delta)$ denotes the probability distribution function. For temperature decrease, $u_{ij}$ is built as follows:

$$u_{ij} = 1 - F(\delta_{ij}) = \int_{\delta_{ij}}^{+\infty} f_i(\delta) \mathrm{d}\delta. \tag{2}$$

According to the definition of information entropy, the temperature entropy (TE) of $\delta_{ij}$ is expressed by $S_{ij}$ as follows:

$$S_{ij} = -\left[u_{ij} \ln u_{ij} + (1 - u_{ij}) \ln(1 - u_{ij})\right] = -\sum_{k=1}^{2} u_{ij}^{p} \ln u_{ij}^{p}, \tag{3}$$

where $p$ is a parameter with a value of one or two, and $u_{ij}^{1} = u_{ij}$ and $u_{ij}^{2} = 1 - u_{ij}$ are the order degree and the disorder degree of $\delta_{ij}$, respectively. Obviously, the disorder degree decreases while the order degree increases and vice versa.

This work regards the temperature field of high concrete dams as an interactional system in which characteristic points have different contribution degrees. $\omega_i$ is used to describe the contribution degree of the $i$th point. The weight entropy (WE) $S_\omega$ is established as follows:

$$S_\omega = -\sum_{i=1}^{n} \omega_i \ln \omega_i. \tag{4}$$

Information entropy and weight parameters are combined to describe the distribution characteristics of the temperature field. Then, TFE can be constructed as follows:

$$\begin{aligned} S_j &= -\sum_{i=1}^{n} \sum_{p=1}^{2} \omega_i u_{ij}^{p} \ln\left(\omega_i u_{ij}^{p}\right) \\ &= -\sum_{i=1}^{n} \sum_{p=1}^{2} \omega_i u_{ij}^{p} \left(\ln \omega_i + \ln u_{ij}^{p}\right) \\ &= -\sum_{i=1}^{n} \sum_{p=1}^{2} \omega_i u_{ij}^{p} \ln \omega_i - \sum_{i=1}^{n} \sum_{p=1}^{2} \omega_i u_{ij}^{p} \ln u_{ij}^{p} \\ &= -\sum_{i=1}^{n} \omega_i \ln \omega_i \sum_{p=1}^{2} u_{ij}^{p} - \sum_{i=1}^{n} \omega_i \sum_{p=1}^{2} u_{ij}^{p} \ln u_{ij}^{p} \\ &= S_\omega + \sum_{i=1}^{n} \omega_i S_{ij} \end{aligned} \tag{5}$$

Equation (5) reveals that TFE involves WE and the weighted TE. The lower the quantity of TFE, the more dangerous the temperature status demonstrates.

### *2.2. Weight Optimization*

PPA, as a high-dimensional data analysis method, can identify data structures and characteristics by projecting high-dimensional monitoring data into a low-dimensional

space. PPA [47–50] is used to optimize the weight parameters. The calculation steps are given as follows.

Calculate $S_{ij}$ by using Equations (1)–(3). The matrix $S$ is constructed as follows:

$$S = \{S_{ij}\} = \begin{Bmatrix} S_{11} & S_{12} & \cdots & S_{1m} \\ S_{21} & S_{22} & \cdots & S_{2m} \\ \vdots & \vdots & \ddots & \vdots \\ S_{n1} & S_{n2} & \cdots & S_{nm} \end{Bmatrix}, \tag{6}$$

where $m$ is the total number of observation dates, and $n$ denotes the total number of observation points. Project $\boldsymbol{S}$ to the unit direction $\boldsymbol{P} = \{p_1, p_2, \cdots, p_j, \cdots, p_n\}$, where ${p_1}^2 + {p_2}^2 + \cdots + {p_n}^2 = 1$. The projection function $G(i)$ is expressed as follows:

$$G(i) = \sum_{j=1}^{m} p_j \cdot S_{ij}. \tag{7}$$

The best projection direction $\boldsymbol{P}^*$ is determined by solving the following optimization problem, namely:

$$\text{Max} : H(p) = S_G \cdot Q_G \tag{8}$$

$$\text{Constraint} : \sum_{j=1}^{m} {p_j}^2 = 1. \tag{9}$$

In Equation (8), $S_G$ and $Q_G$ are expressed as follows:

$$S_G = \sqrt{\frac{\sum_{i=1}^{n} [G(i) - \overline{g}(i)]^2}{n-1}} \tag{10}$$

$$Q_G = \sum_{i=1}^{n} \sum_{j=1}^{m} (R - r_{ij}) \cdot f(R - r_{ij}), \tag{11}$$

where $\overline{g}(i)$ is the mean value of $G(i)$, $R = 0.1S_G$, $r_{ij} = |G(i) - G(j)|$ is the distance between $G(i)$ and $G(j)$, and $f(t)$ is a unit step function equal to 1 if $t > 0$; otherwise, it is 0. Substitute $\boldsymbol{P}^*$ into Equation (7) to compute $G^*(i)$. Then, calculate the individual contribution $\omega_i$ by using the following:

$$\omega_i = \frac{G^*(i)}{\sum_{i=1}^{n} G^*(i)}. \tag{12}$$

## 3. Temperature Control Index Construction Based on Cloud Model

### *3.1. Cloud Model Algorithm*

Here, $U$ denotes a domain, $C$ is a qualitative concept, $x \in U$ is a variable, and the certainty degree of $x$ is recorded as $u$, a random number in the range of [0, 1]. The distribution of $x$ on $U$ is called a cloud, and the point $(x, u)$ is a cloud droplet.

The mathematical features of cloud model, i.e., the expectation $E_x$, the entropy $E_n$, and the hyper entropy $H_e$, are calculated by using reverse cloud generator. For a data set $x = \{x_1, x_2, \cdots, x_l, \cdots, x_k\}$, $k$ is its data size, and the mean value $\overline{x}$ and the variance $\sigma_x$ are calculated as follows:

$$\overline{x} = \frac{1}{k} \sum_{l=1}^{k} x_l \tag{13}$$

$$\sigma_x = \sqrt{\frac{1}{k-1} \sum_{l=1}^{k} (x_l - \overline{x})^2}. \tag{14}$$

The calculation expressions of $E_x$, $E_n$, and $H_e$ are as follows:

$$E_x = \overline{x}, \tag{15}$$

$$E_n = \left(\frac{\pi}{2}\right)^{1/2} \frac{1}{k} \sum_{l=1}^{k} |x_l - E_x|, \tag{16}$$

$$H_e = \sqrt{{\sigma_x}^2 - {E_n}^2}. \tag{17}$$

Cloud droplets are generated by using a forward cloud generator. The algorithm steps are as follows [51–55]. Generate the normal random number ${E'}_{n_i}$ with the mean value of $E_n$ and the variance of ${H_e}^2$, expressed as follows:

$${E'}_{n_i} = NORM\left(E_n, {H_e}^2\right). \tag{18}$$

Build the normal random number $x_i$ with the mean value of $E_x$ and the variance of ${E'}_{n_i}$, recorded as follows:

$$x_i = NORM\left(E_x, {E'}_{n_i}\right). \tag{19}$$

The certainty degree $u_i$ of $x_i$ is calculated as follows:

$$u_i = e^{-\frac{(x_i - E_x)^2}{2{E'}_{n_i}}}. \tag{20}$$

Repeat the above steps, and all preset cloud droplets can be generated. The upper and lower bounds of cloud droplets are expressed by $y^u(x)$ and $y^l(x)$ as follows:

$$y^u(x) = e^{-\frac{(x - E_x)^2}{2(E_n + 3H_e)^2}} \tag{21}$$

$$y^l(x) = e^{-\frac{(x - E_x)^2}{2(E_n - 3H_e)^2}}. \tag{22}$$

The three mathematical features have different impacts on the morphology of artificial clouds. If artificial clouds have the same values of $E_n$ and $H_e$ but different $E_x$, then their dispersion degrees, distribution ranges, and cloud thickness are basically the same. However, the center areas are different, as shown in Figure 2a,b. If artificial clouds have the same values of $H_e$ and $E_x$ but different $E_n$, then their center areas and cloud thickness are similar, while the dispersion degrees and distribution ranges are different, as shown in Figure 2a,c. Moreover, it can be seen from Figure 2a,d that same $E_x$, same $E_n$, and different $H_e$ result in similar center areas, similar dispersion degrees, similar distribution ranges, but different cloud thickness. The greater the value of $H_e$, the thicker the artificial cloud exhibits.

### *3.2. Temperature Control Index*

Table 1 shows the contribution degrees of different domains, which are important references to establish the temperature control index. Considering practical situations of high concrete dams, TFEs under unfavorable conditions are taken as samples, and the data set $S'$ is constructed as follows:

$$S' = \{S_1, S_2, \cdots, S_k\}. \tag{23}$$

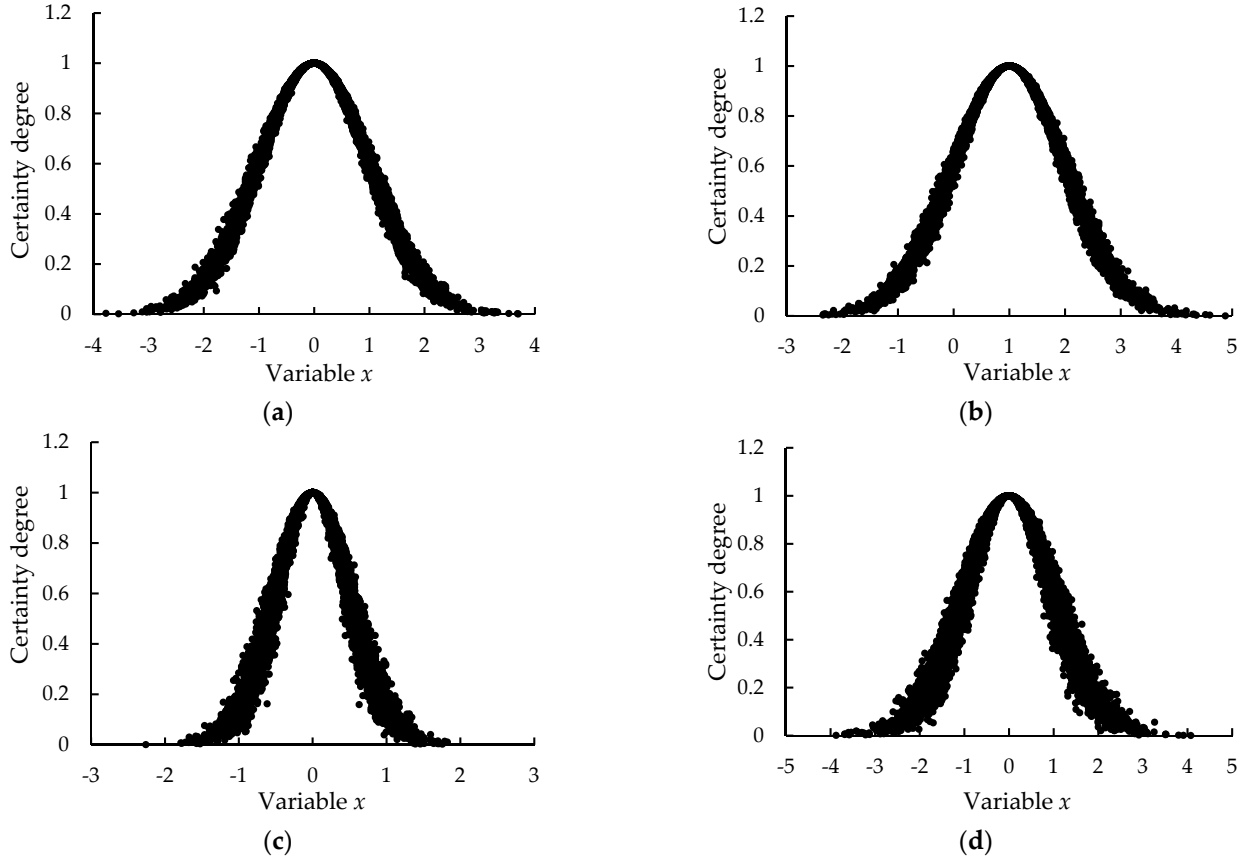


**Figure 2.** Cloud droplet distributions with different mathematical features: (**a**) $E_x = 0$, $E_n = 1$, and $H_e = 0.05$; (**b**) $E_x = 1$, $E_n = 1$, and $H_e = 0.05$; (**c**) $E_x = 0$, $E_n = 0.5$; and $H_e = 0.05$; and (**d**) $E_x = 0$, $E_n = 1$, and $H_e = 0.1$.

**Table 1.** The $\Delta D$ and $\beta$ values of $\Delta U$.

| Domain $\Delta U$ | Contribution Degree $\Delta D$ | Value of $\beta$ |
|---|---|---|
| $[E_x - 0.67E_k, E_x + 0.67E_k]$ | 50.0% | 0.67 |
| $[E_x - E_k, E_x + E_k]$ | 68.3% | 1.00 |
| $[E_x - 1.96E_k, E_x + 1.96E_k]$ | 95.0% | 1.96 |
| $[E_x - 2E_k, E_x + 2E_k]$ | 95.5% | 2.00 |
| $[E_x - 2.58E_k, E_x + 2.58E_k]$ | 99.0% | 2.58 |
| $[E_x - 3E_k, E_x + 3E_k]$ | 99.7% | 3.00 |

$E_x$, $E_n$, and $H_e$ are calculated by employing the reverse cloud generator, and cloud droplets are generated using the forward cloud generator. $\alpha$ denotes the confidence level. The relationship between the confidence level $\alpha$ and the contribution degree $\Delta D$ is $\alpha = 1 - \Delta D$. According to the principle of small probability event, if small probability events occur, then the studied dam is in different degrees of abnormality. The corresponding temperature control index $S_{m,\alpha}$ is constructed as follows:

$$S_{m,\alpha} = E_x - \beta E_n, \tag{24}$$

where $\beta$ is a parameter related to $\alpha$. According to Table 1, if $\alpha$ is set as 0.01, then $\beta$ equals 2.58. Dam security can be evaluated by comparing $S_j$ and $S_{m,\alpha}$. If $S_j < S_{m,\alpha}$, then the studied dam may be in an abnormal state on the $j$th observation date. Appropriate measures should be taken to improve the temperature state of the studied dam.

In actual applications, several confidence levels $\alpha_1, \alpha_2, \cdots, \alpha_k$ ($\alpha_1 > \alpha_2 > \cdots > \alpha_k$) are set, and the corresponding $S_{m,\alpha_1}, S_{m,\alpha_2}, \cdots, S_{m,\alpha_k}$ ($S_{m,\alpha_1} < S_{m,\alpha_2} < \cdots < S_{m,\alpha_k}$) are

used for multi-level dam risk management. It should be noted that $\alpha$ is determined by considering various factors, e.g., engineering and build grades. This parameter should be carefully selected.

The algorithm flowchart is shown in Figure 3.

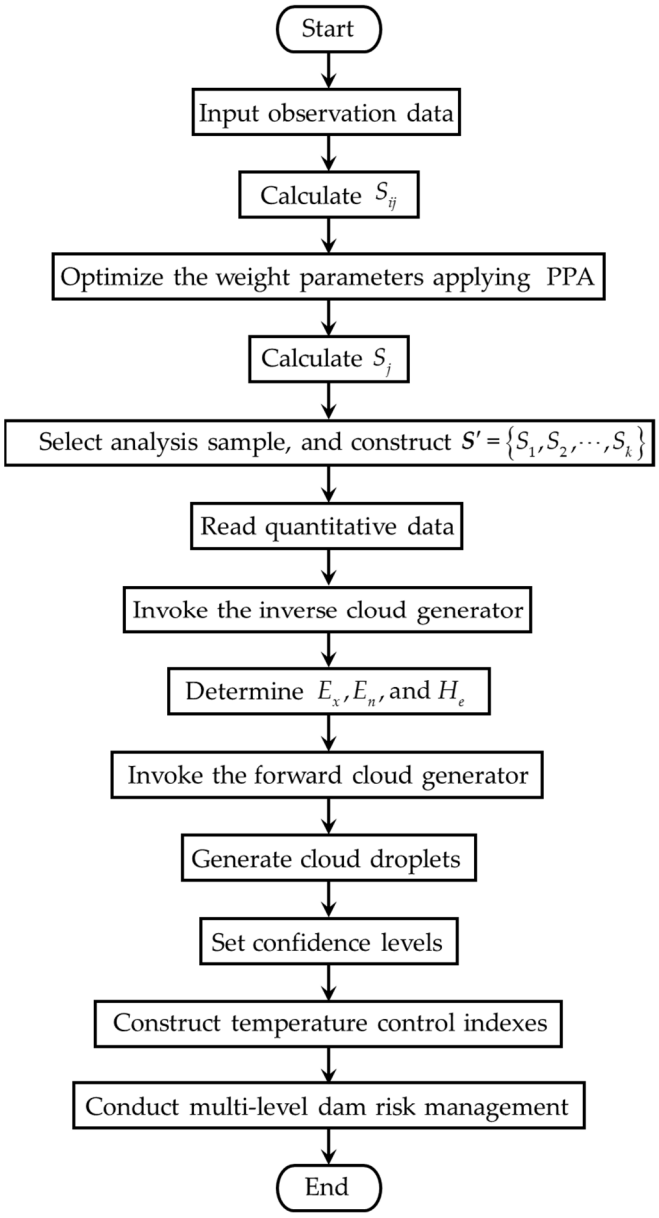


**Figure 3.** Algorithm flowchart.

## 4. Case Study

### *4.1. In Situ Observation Data*

The studied dam is a RCC gravity dam, and it is located on the Jinsha River in southwestern China. This dam has a crest elevation of 1424.00 m, a maximum dam height of 160.00 m, and a crest length of 640.00 m. The storage capacity of the reservoir is $9.13 \times 10^9$ m$^3$. The normal and checked water levels are 1418.00 m and 1421.07 m, respectively. The proposed methodology is adopted for the #6 dam section. Thirty-three observation points are installed to monitor temperature variations, as shown in Figure 4. Figure 5 gives the time curves of air temperature that show a periodic change pattern. Taking November 2011 as an example, the average daily temperature is 14.2 °C, the maximum temperature is 30.7 °C, and the minimum temperature is 4.7 °C. The average, maximum,

and minimum temperature differences between day and night are 17.4 °C, 22.5 °C, and 7.4 °C, respectively.

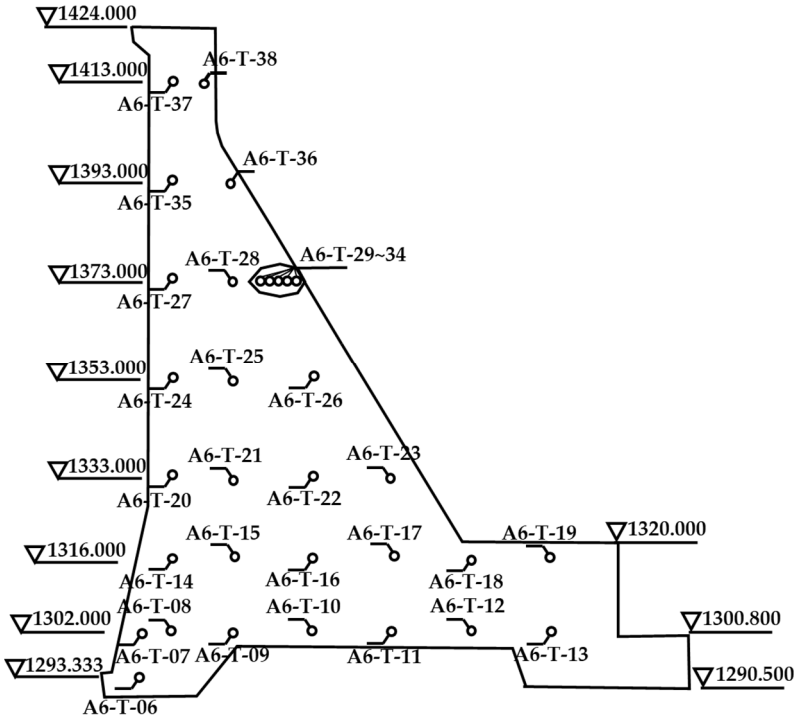


**Figure 4.** Distribution of the 33 observation points.

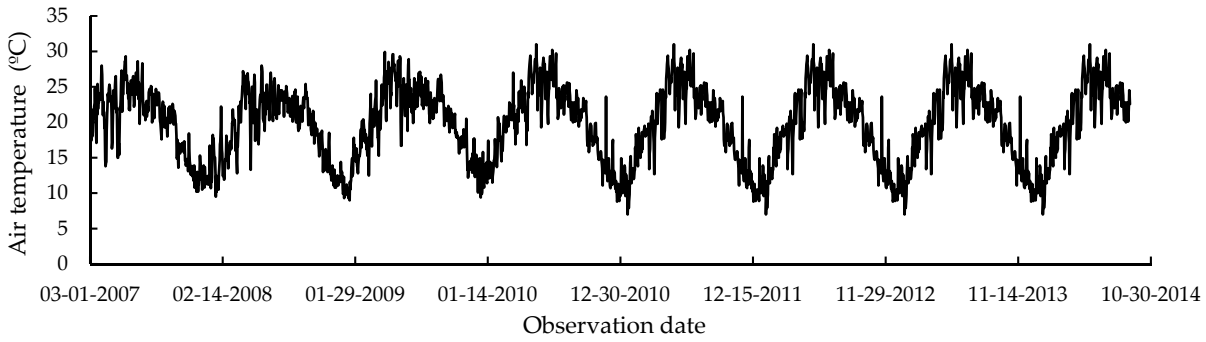


**Figure 5.** Time curves of air temperature.

The time curve of the concrete temperature observed at A6-T-21 is shown in Figure 6. In the early stage of concrete pouring, the concrete temperature gradually increases due to cement hydration heat. As cement hydration heat gradually dissipates, the concrete temperature exhibits a decreasing trend. Figure 7a,b show the temperature field distributions before and after water storage, respectively. After the upstream water level reaches 1397.83 m, the temperature change on the upstream surface is mainly affected by air temperature and water temperature. Compared with the downstream surface, the change amplitude of the upstream surface is relatively smaller. It can be seen from Table 2 that the maximum and minimum values are 49.4 °C and 12.4 °C, respectively, and that the maximum annual variation is 22.0 °C, which appeared at A6-T-37 in 2009.

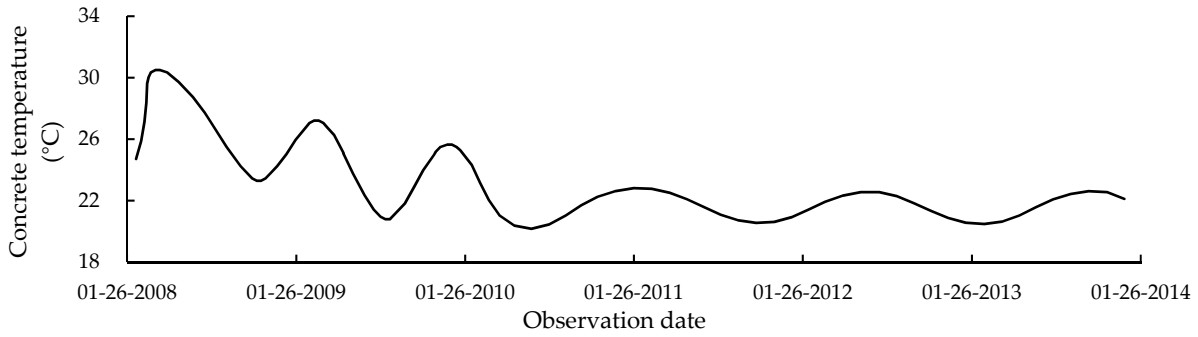


**Figure 6.** Time curve of concrete temperature observed at A6-T-21.

**Table 2.** Maximum value, minimum value, and maximum annual variation.

| Observation Point | Point Number | Maximum Value/ Date (mm-dd-yyyy) | Minimal Value/ Date (mm-dd-yyyy) | Maximum Annual Variation/Year (yyyy) |
|---|---|---|---|---|
| A6-T-06 | 1 | 31.1/09-11-2007 | 17.0/08-30-2007 | 14.2/2007 |
| A6-T-07 | 2 | 31.9/10-22-2008 | 20.0/01-30-2012 | 10.8/2008 |
| A6-T-08 | 3 | 34.0/09-05-2008 | 23.0/02-01-2010 | 10.9/2008 |
| A6-T-09 | 4 | 33.0/09-10-2008 | 17.9/03-11-2008 | 15.1/2008 |
| A6-T-10 | 5 | 30.8/05-12-2008 | 17.4/03-11-2008 | 13.5/2008 |
| A6-T-11 | 6 | 34.6/10-07-2008 | 19.9/02-22-2012 | 11.3/2008 |
| A6-T-12 | 7 | 40.6/05-19-2008 | 22.2/03-22-2008 | 18.4/2008 |
| A6-T-13 | 8 | 33.8/09-02-2008 | 18.1/02-01-2010 | 15.0/2008 |
| A6-T-14 | 9 | 30.4/06-06-2008 | 18.1/08-19-2010 | 10.3/2008 |
| A6-T-15 | 10 | 30.5/07-04-2008 | 17.4/01-03-2011 | 10.3/2008 |
| A6-T-16 | 11 | 32.3/05-23-2008 | 19.9/08-11-2011 | 11.8/2008 |
| A6-T-17 | 12 | 31.7/05-16-2008 | 18.5/03-18-2011 | 11.8/2008 |
| A6-T-18 | 13 | 31.5/05-16-2008 | 20.7/12-28-2011 | 10.9/2008 |
| A6-T-19 | 14 | 31.7/05-16-2008 | 19.6/04-19-2008 | 12.2/2008 |
| A6-T-20 | 15 | 37.7/05-17-2008 | 14.7/12-28-2011 | 18.9/2008 |
| A6-T-21 | 16 | 37.1/08-15-2008 | 17.9/05-05-2008 | 19.2/2008 |
| A6-T-22 | 17 | 35.5/08-29-2008 | 18.1/05-05-2008 | 17.4/2008 |
| A6-T-23 | 18 | 32.1/06-06-2008 | 18.6/05-05-2008 | 13.5/2008 |
| A6-T-24 | 19 | 38.0/07-24-2008 | 19.0/07-03-2008 | 19.0/2008 |
| A6-T-25 | 20 | 34.2/09-05-2008 | 19.0/07-03-2008- | 15.3/2008 |
| A6-T-26 | 21 | 30.5/02-11-2010 | 20.0/07-03-2008 | 10.5/2008 |
| A6-T-27 | 22 | 31.7/01-14-2009 | 12.4/03-10-2011 | 10.6/2008 |
| A6-T-28 | 23 | 28.5/12-17-2010 | 18.3/12-03-2008 | 5.9/2008 |
| A6-T-29 | 24 | 28.4/08-11-2010 | 19.0/12-03-2008 | 4.9/2008 |
| A6-T-30 | 25 | 40.2/11-05-2009 | 18.1/12-03-2008 | 14.3/2009 |
| A6-T-31 | 26 | 32.0/12-17-2010 | 18.6/12-03-2008 | 5.8/2010 |
| A6-T-32 | 27 | 31.8/12-17-2010 | 18.0/12-03-2008 | 6.3/2008 |
| A6-T-33 | 28 | 27.9/12-17-2010 | 17.8/12-03-2008 | 6.9/2008 |
| A6-T-34 | 29 | 30.5/08-26-2010 | 14.0/12-04-2008 | 7.8/2010 |
| A6-T-35 | 30 | 49.4/05-28-2009 | 17.3/07-22-2011 | 21.2/2009 |
| A6-T-36 | 31 | 39.6/05-28-2009 | 17.5/01-20-2011 | 20.6/2009 |
| A6-T-37 | 32 | 48.5/10-04-2009 | 19.0/04-06-2011 | 22.0/2009 |
| A6-T-38 | 33 | 45.3/09-28-2009 | 22.4/02-10-2012 | 16.5/2009 |

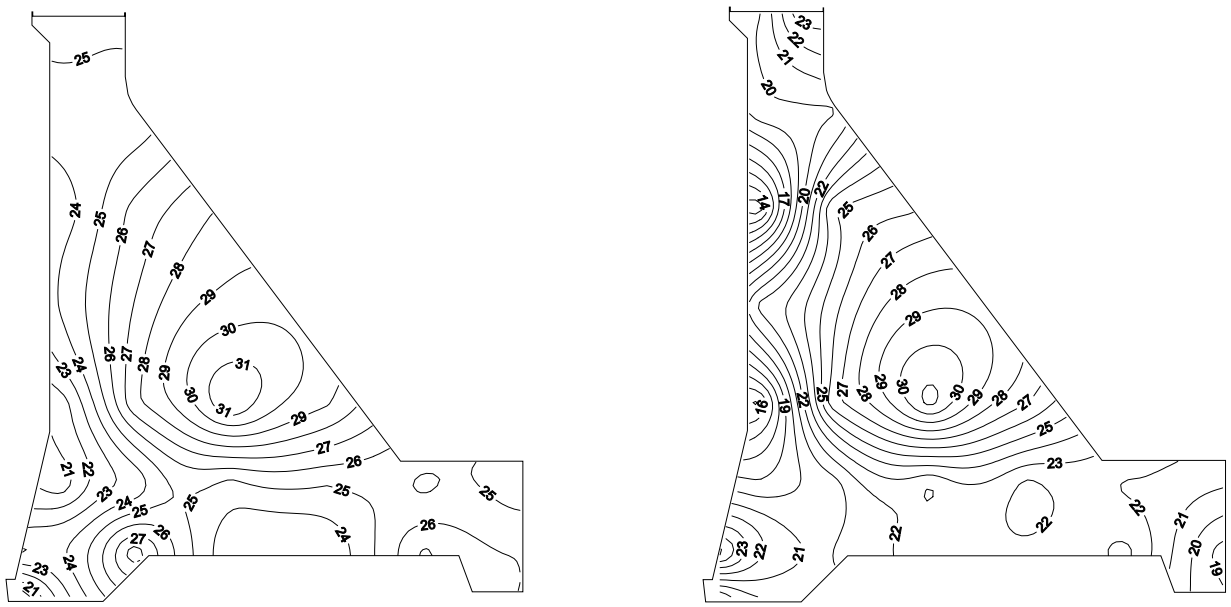

(**a**) (**b**)

**Figure 7.** Temperature field distributions, (**a**) before water storage and (**b**) after water storage.

### *4.2. Weight Distribution*

The concrete pouring of the #6 dam section began on 29 July 2007. The construction was completed on 16 November 2009. The dam foundation elevation is 1288.00 m, and the dam crest elevation is 1424.00 m. The average pouring temperature is approximately 16 °C. The analysis period is divided into four stages according to the pouring process. Stage 1 is from 26 January 2008 to 6 March 2008. The corresponding pouring elevation is 1311.00 m. Stage 2 is from 7 March 2008 to 10 August 2008 with a pouring elevation of 1360.00 m. Stage 3 is from 11 August 2008 to 26 November 2009, and the pouring elevation is 1422.50 m. Stage 4 is from 27 November 2009 to 20 January 2014. At this stage, the dam construction has been completed. The weight distribution is optimized by PPA, and the results are shown in Figure 8. The point numbers are given in Table 2. To verify the reasonability of the weight distribution, the temperature fields of the four stages are simulated using the FE method. The numerical simulation considers the comprehensive effects of cement hydration heat, ambient temperature, and cooling water pipes. The initial temperature of cooling water is approximately 11.4 °C. Figure 9a,b show the FE models of the dam body, foundation, and cooling water pipe. The ABAQUS 2021 software is used to conduct numerical simulations in this work. The temperature distributions are presented in Figure 10a–d. Apparently, observation points with higher calculation values have higher weight parameters, indicating that the weight distribution patterns are in line with actual situations.

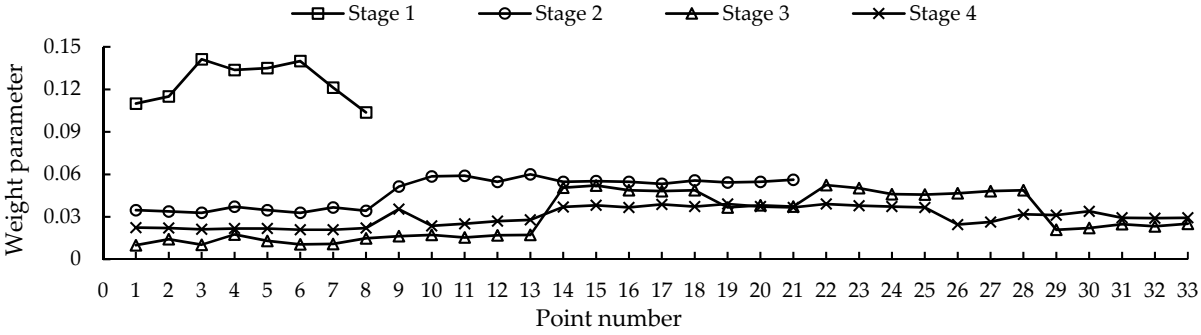


**Figure 8.** Weight distribution.

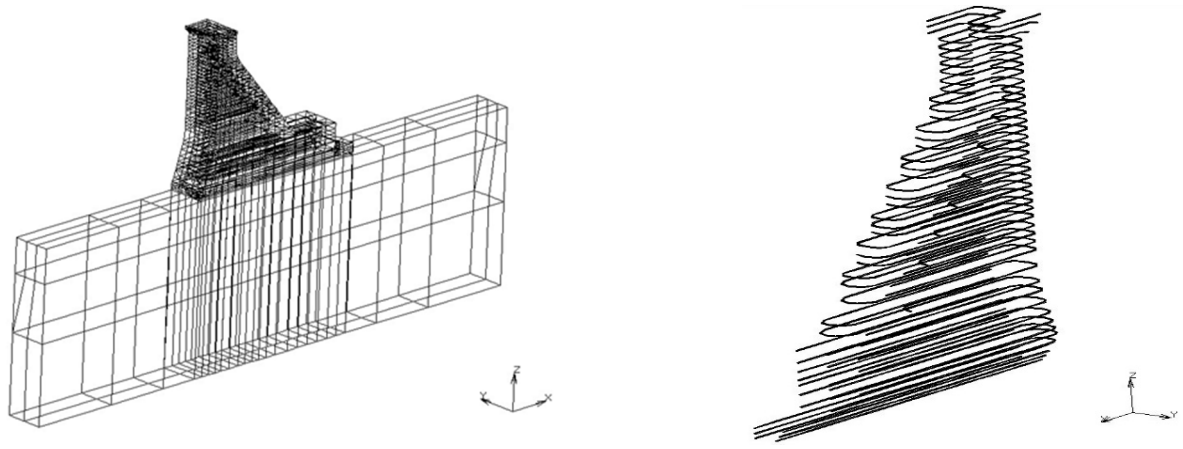

(**a**) (**b**)

**Figure 9.** The established FE models. (**a**) The dam body and foundation, and (**b**) the cooling water pipe.

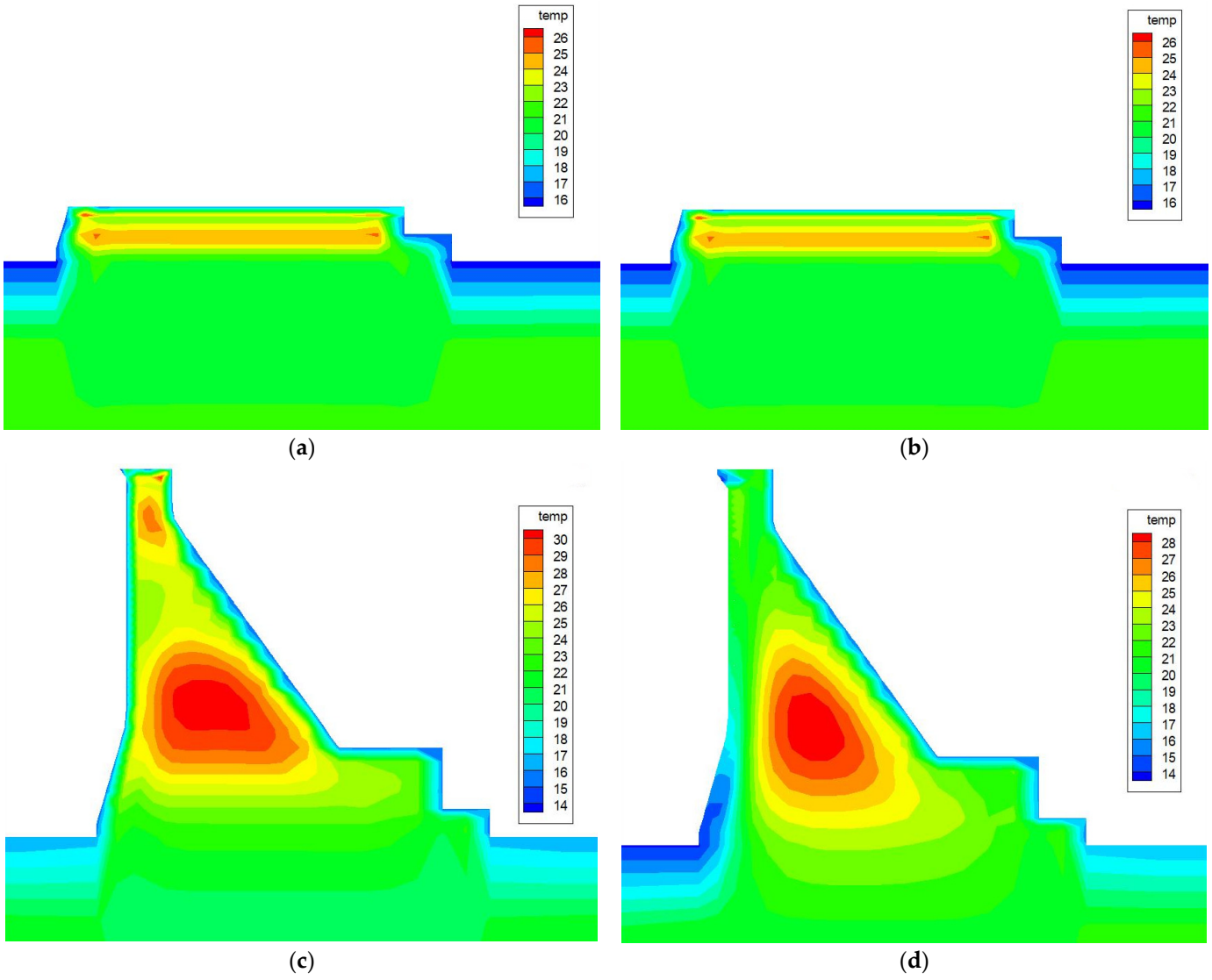


(**a**) (**b**)

(**c**) (**d**)

**Figure 10.** Simulation results of temperature fields: (**a**) pouring elevation at 1311.00 m; (**b**) pouring elevation at 1360.00 m; (**c**) pouring elevation at 1422.50 m; and (**d**) 4 years after completion.

### *4.3. Comparative Analysis*

At an early stage of the construction period, concrete materials release abundant heat, and dam temperature quickly increases, leading to a decrease in TFEs. Thereafter, the concrete temperature of the dam body gradually decreases due to artificial cooling and heat dissipation, leading to an increase in TFEs. Since the end of Stage 3, the concrete temperature of the dam body has started to decrease and tends to stabilize gradually. Due to periodic changes in ambient temperature, TFEs show periodic fluctuations at Stage 4, as demonstrated in Figure 11. The regularities of TFEs agree with actual situations, and Equation (5) can effectively characterize the evolution characteristics of a high concrete dam temperature field.

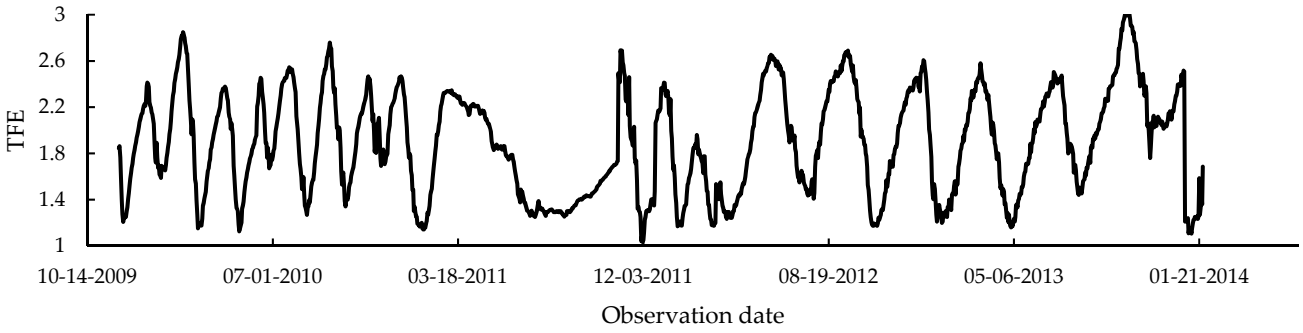


**Figure 11.** Time curve of TFEs for the #6 dam section.

In this work, the typical small probability method is compared with the cloud model. The analysis process is as follows. The probability distribution of $S' = \{S_1, S_2, \cdots, S_k\}$ is tested by the Kolmogorov–Smirnov (K–S) method [56,57]. Then, its probability density function $f(S)$ and distribution function $F(S)$ are determined. According to the confidence level $\alpha$, its abnormal probability is expressed by $P(S \leq S_{m,\alpha})$ as follows:

$$P(S \leq S_{m,\alpha}) = \int_{-\infty}^{S_{m,\alpha}} f(S)\mathrm{d}x. \tag{25}$$

Then, the control index value $S_{m,\alpha}$ is established as follows:

$$S_{m,\alpha} = F^{-1}(\overline{S}, \sigma_S, \alpha), \tag{26}$$

where $\overline{S}$ and $\sigma_S$ denote the mean value and the variance of $S'$, respectively. The two parameters are calculated by Equations (13) and (14). The annual extreme values of $S_j$ are listed in Table 3. The results of the K–S test are shown in Table 4, and the most reasonable probability distribution is the normal distribution with $\overline{S} = 1.14$ and $\sigma_S = 0.0589$. For the cloud model, the values of $E_x$, $E_n$, and $H_e$ are 1.1400, 0.0501, and 0.0070, respectively, and the values of $\beta$ are 1.96 ($\alpha = 5\%$) and 2.58 ($\alpha = 1\%$), respectively. The distribution of cloud droplets is shown in Figure 12. This paper sets two control levels according to different dangerous situations, i.e., Level 1 ($\alpha = 5\%$) and Level 2 ($\alpha = 1\%$). The calculated results of the typical small probability method and the cloud model are listed in Table 5. Their results are relatively consistent, indicating that the constructed indexes are reasonable and credible. Moreover, the cloud model, compared with the typical small probability method, also has the advantage that it can still obtain high-precision control indexes in the case of small samples.

**Table 3.** Annual extreme values.

| Year | 2008 | 2009 | 2010 | 2011 | 2012 | 2013 |
|---|---|---|---|---|---|---|
| Minimum value of TFEs | 0.723 | 0.968 | 1.126 | 1.034 | 1.170 | 1.160 |

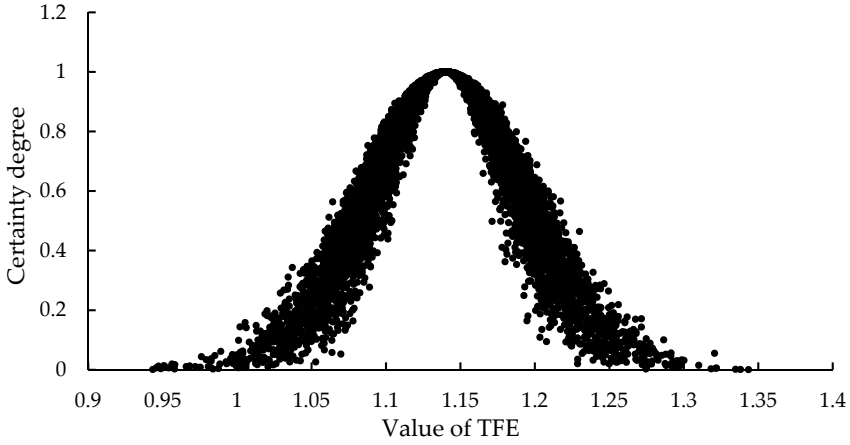


**Figure 12.** Distribution of cloud droplets.

**Table 4.** K–S test results.

| Probability Distribution | Confidence Level |
|---|---|
| Lognormal distribution | 0.23 |
| Normal distribution | 0.15 |
| Uniform distribution | 0.64 |
| Triangular distribution | 0.33 |
| Exponential distribution | 0.41 |
| $\gamma$ distribution | 0.87 |
| $\beta$ distribution | 0.78 |

**Table 5.** Temperature control indexes of the two methods.

| Method | Temperature Control Index | |
|---|---|---|
| Typical small probability method | $\alpha = 5\%$<br>1.0431 | $\alpha = 1\%$<br>1.0031 |
| Cloud model | $\alpha = 5\%$<br>1.0418 | $\alpha = 1\%$<br>1.0107 |

According to the above analyses, the established control indexes are appropriate for global monitoring of temperature fields, whereas conventional indexes are appropriate for local monitoring. Given that global monitoring is more important than local monitoring, the established indexes have greater significance than conventional indexes. This research offers scientific reference and technical support for the temperature control of other similar high concrete dam projects.

## 5. Conclusions and Suggestions

This work establishes the temperature control indexes for high concrete dams from the perspective of the spatial field. Information entropy theory is applied to describe the evaluation regularity of the temperature field, and then the expression of TFE that considers the contribution degrees of different observation points is established. Using TFE, the cloud model is employed to build the temperature control indexes. A case study is conducted in which the cloud model is compared with the typical small probability method. According to the calculation results, the variation law of TFEs agrees with actual situations, and the determined temperature control indexes can improve the safety management level of high concrete dams. Based on actual situations, different temperature control measures can be taken, e.g., pre-cooling methods such as lowering the temperature of concrete-forming components or post-cooling methods like running cold water through a pipe embedded in dam concrete.

Through contrastive analysis, the following conclusions can be drawn. When using the typical small probability method, the probability distribution of dangerous observation values needs to be determined. It is not applicable when the observation time is short. If the analysis samples do not conform to a definite distribution, then the applicability of this method is greatly limited. The cloud model directly obtains the mathematical features using the reverse cloud generator and generates cloud droplets by employing the forward cloud generator. As a result, this model can effectively represent the characteristics of a pan-normal distribution, and it has wider application conditions than the typical small probability method. Moreover, the cloud model considers the randomness and fuzziness of information, and no strict requirements are put on the sample size. Therefore, there is no need to test the probability distribution of the analysis example. In addition, it should be noted that this case study sets two confidence levels, i.e., $\alpha = 1\%$ and 5%. In fact, there is no unified standard for selecting the values of $\alpha$. The determination of $\alpha$ should be given full consideration to practical experience and theoretical calculation, and detailed arguments need to be conducted.

**Author Contributions:** Detailed author contributions of this research are listed as follows. Conceptualization, G.Y., B.L. and J.S.; methodology, G.Y., J.S. and B.L.; software, B.L. and J.Z.; investigation, Z.H. and A.Z.; formal analysis, J.Z.; resources, Z.H. and A.Z.; writing-original draft preparation, G.Y. and J.S.; writing-review and editing, J.S. and J.N. All authors have read and agreed to the published version of the manuscript.

**Funding:** This research is supported by the National Natural Science Foundation of China (grant numbers 52109155 and 52279133), the Scientific Research Foundation of high-level talents of the North China University of Water Resources and Electric Power (grant number 202005017), and the Belt and Road Special Foundation of the State Key Laboratory of Hydrology-Water Resources and Hydraulic Engineering (grant number 2019492211).

**Data Availability Statement:** The data used to support the findings of this study are available from the corresponding authors upon request.

**Acknowledgments:** I am grateful to Hohai University. In addition, I thank Chongshi Gu and Hao Gu for their precious suggestions.

**Conflicts of Interest:** The authors declare that they have no known competing financial interest or personal relationship that could have appeared to influence the work reported in this paper.

## Nomenclature and Abbreviations

**Nomenclature**

| | |
|---|---|
| $i$ | an observation point |
| $j$ | an observation date |
| $\delta_{ij}$ | the observation value of the $i$th point on the $j$th date |
| $u_{ij}$ | a parameter related to the order degree |
| $p$ | a parameter related to $u_{ij}^1$ and $u_{ij}^2$ |
| $u_{ij}^1$ | the order degree of $\delta_{ij}$ |
| $u_{ij}^2$ | the disorder degree of $\delta_{ij}$ |
| $f_i(\delta)$ | the probability density function of $\delta_{ij}$ |
| $F_i(\delta)$ | the probability distribution function of $\delta_{ij}$ |
| $S_{ij}$ | the temperature entropy of $\delta_{ij}$ |
| $\omega_i$ | the weight of the $i$th point |
| $S_j$ | the TFE on the $j$th date |
| $S$ | a matrix |
| $m$ | the total number of observation dates |
| $n$ | the total number of observation points |
| $\boldsymbol{P}$ | the unit projection direction |
| $G(i)$ | the projection function |
| $\boldsymbol{P}^*$ | the best projection direction |
| $\overline{g}(i)$ | the mean value of $G(i)$ |

| | |
|---|---|
| $S_G$ | a parameter related to PPA |
| $Q_G$ | a parameter related to PPA |
| $G^*(i)$ | a parameter related to $\boldsymbol{P}^*$ |
| $R$ | a parameter related to PPA |
| $r_{ij}$ | the distance between $G(i)$ and $G(j)$ |
| $f(t)$ | a unit step function |
| $t$ | a parameter related to $f(t)$ |
| $U$ | the domain |
| $C$ | a qualitative concept |
| $x$ | a variable |
| $u$ | the certainty degree of $x$ |
| $E_x$ | the expectation of the cloud model |
| $E_n$ | the entropy of the cloud model |
| $H_e$ | The hyper entropy of the cloud model |
| $\boldsymbol{x}$ | a data set |
| $\overline{x}$ | the mean value of $\boldsymbol{x}$ |
| $\sigma_x$ | the variance of $\boldsymbol{x}$ |
| $\boldsymbol{S}'$ | a data set |
| $f(S)$ | the probability density function of $\boldsymbol{S}'$ |
| $F(S)$ | the distribution function of $\boldsymbol{S}'$ |
| $P$ | the abnormal probability |
| $\overline{\boldsymbol{S}}$ | the mean value of $\boldsymbol{S}'$ |
| $\sigma_S$ | the variance of $\boldsymbol{S}'$ |
| $k$ | the size of the data sets $\boldsymbol{x}$ and $\boldsymbol{S}'$ |
| $y^u$ | the upper bounds of cloud droplets |
| $y^l$ | the lower bounds of cloud droplets |
| $\Delta U$ | a micro-interval in the domain $U$ |
| $\Delta D$ | the contribution degree of $\Delta U$ |
| $U_{\Delta U}$ | the certainty degree of $\Delta U$ |
| $\alpha$ | the confidence level |
| $S_{m,\alpha}$ | the temperature control index with a confidence level of $\alpha$ |
| $\beta$ | a parameter related to $\alpha$ |
| **Abbreviations** | |
| PPA | projection pursuit analysis |
| TFE | temperature field entropy |
| FE | finite element |
| RCC | roller compacted concrete |
| TE | temperature entropy |
| WE | weight entropy |
| K-S | Kolmogorov–Smirnov |

## References


1. Sevieri, G.; De Falco, A. Dynamic structural health monitoring for concrete gravity dams based on the Bayesian inference. *J. Civ. Struct. Health Monit.* **2020**, *10*, 235–250. [CrossRef]
2. Shao, C.; Gu, C.; Yang, M.; Xu, Y.; Su, H. A novel model of dam displacement based on panel data. *Struct. Control Health Monit.* **2018**, *25*, e2037. [CrossRef]
3. Zhou, Y.; Bao, T.; Shu, X.; Li, Y.; Li, Y. BIM and ontology-based knowledge management for dam safety monitoring. *Automat. Constr.* **2023**, *145*, 104649. [CrossRef]
4. Hou, C.; Chai, D.; Cheng, H.; Ning, S.; Yang, B.; Zhou, Y. Simulation Feedback of Temperature Field of Super-High Arch Dam during Operation and Its Difference with Design Temperature. *Water* **2022**, *14*, 4028. [CrossRef]
5. Peng, H.; Lin, P.; Xiang, Y.; Hu, J.; Yang, Z. Effects of Carbon Thin Film on Low-Heat Cement Hydration, Temperature and Strength of the Wudongde Dam Concrete. *Buildings* **2022**, *12*, 717. [CrossRef]
6. Qiu, H.; Hu, T.; Zhang, S.; Xiao, Y. Deriving Operating Rules of Hydropower Reservoirs Using Multi-Strategy Ensemble Henry Gas Solubility Optimization-Driven Support Vector Machine. *Water* **2023**, *15*, 437. [CrossRef]
7. Lou, S.; Mo, L.; Zhou, J.; Wang, Y.; He, W. Supply and Demand Forecasting of Water Resource Coupling System in Upstream Yangtze River under Changing Environmental Conditions. *Water* **2021**, *13*, 640. [CrossRef]
8. Pan, J.; Wang, J. Effect of abutment movements on nonlinear seismic response of an arch dam. *Struct. Infrastruct. Eng.* **2019**, *16*, 1106–1120. [CrossRef]

9. Brown, E.T. Reducing risks in the investigation, design and construction of large concrete dams. *J. Rock. Mech. Geotech.* **2017**, *9*, 197–209. [CrossRef]
10. Ahmadi, S.M.; Yamamoto, Y. A New Dam-Break Outflow-Rate Concept and Its Installation to a Hydro-Morphodynamics Simulation Model Based on FDM (An Example on Amagase Dam of Japan). *Water* **2021**, *13*, 1759. [CrossRef]
11. Xu, W.; Zhou, Q.; Dong, X. SPH–DEM coupling method based on GPU and its application to the landslide tsunami. Part II: Reproduction of the Vajont landslide tsunami. *Acta Geotech.* **2021**, *17*, 2121–2137. [CrossRef]
12. Li, B.; Zhang, Z.; Wang, X.; Liu, X. Investigation on the Debonding Failure Model of Anchored Polyurea Coating under a High-Velocity Water Flow and Its Application. *Sustainability* **2019**, *11*, 1261. [CrossRef]
13. Hariri-Ardebili, M.A.; Mahdavi, G.; Nuss, L.K.; Lall, U. The role of artificial intelligence and digital technologies in dam engineering: Narrative review and outlook. *Eng. Appl. Artif. Intel.* **2023**, *126*, 106813. [CrossRef]
14. Ma, K.; Xu, N.; Liang, Z. Stability Assessment of the Excavated Rock Slope at the Dagangshan Hydropower Station in China Based on Microseismic Monitoring. *Adv. Civ. Eng.* **2018**, *2018*, 4567258. [CrossRef]
15. Ma, K.; Sun, X.; Zhang, Z.; Hu, J.; Wang, Z. Intelligent Location of Microseismic Events Based on a Fully Convolutional Neural Network (FCNN). *Rock. Mech. Rock. Eng.* **2022**, *55*, 4801–4817. [CrossRef]
16. Prakash, G.; Sadhu, A.; Narasimhan, S.; Brehe, J.-M. Initial service life data towards structural health monitoring of a concrete arch dam. *Struct. Control Health Monit.* **2018**, *25*, e2036. [CrossRef]
17. Yosef, T.Y.; Song, C.R.; Chang, K.-T. Hydro-thermal coupled analysis for health monitoring of embankment dams. *Acta Geotech.* **2018**, *13*, 447–455. [CrossRef]
18. Yun, T.; Butler, K.E.; MacQuarrie, K.T.B. Investigation of seepage near the interface between an embankment dam and a concrete structure: Monitoring and modelling of seasonal temperature trends. *Can. Geotech. J.* **2023**, *60*, 453–470. [CrossRef]
19. Song, C.R.; Yosef, T.Y. Seepage Monitoring of an Embankment Dam Based on Hydro-Thermal Coupled Analysis. *J. Eng. Mater. Technol.* **2017**, *139*, 021024. [CrossRef]
20. Din, Z.U.; Ali, A.; De la Sen, M.; Zaman, G. Entropy generation from convective–radiative moving exponential porous fins with variable thermal conductivity and internal heat generations. *Sci. Rep.* **2022**, *12*, 1791. [CrossRef]
21. Xie, Z.; Yu, T. Determination of Monitoring Control Value for Concrete Gravity Dam Spatial Deformation Based on POT Model. *Cmes-Comp. Model. Eng.* **2023**, *135*, 2119–2135. [CrossRef]
22. Zhou, X.; Huang, X.; Zhao, H.; Ma, K. Development of a revised method for indicators of hydrologic alteration for analyzing the cumulative impacts of cascading reservoirs on flow regime. *Hydrol. Earth Syst. Sci.* **2020**, *24*, 4091–4107. [CrossRef]
23. Chen, H.; Liu, Z. Temperature control and thermal-induced stress field analysis of GongGuoQiao RCC dam. *J. Therm. Anal. Calorim.* **2018**, *135*, 2019–2029. [CrossRef]
24. Chen, Z.; Zheng, D.; Li, J.; Wu, X.; Qiu, J.; Nguyen Thanh, N. Temperature Field Online Reconstruction for In-Service Concrete Arch Dam Based on Limited Temperature Observation Data Using AdaBoost-ANN Algorithm. *Math. Probl. Eng.* **2021**, *2021*, 9979994. [CrossRef]
25. Pan, J.; Liu, W.; Wang, J.; Jin, F.; Chi, F. A novel reconstruction method of temperature field for thermomechanical stress analysis of arch dams. *Measurement* **2022**, *188*, 110585. [CrossRef]
26. Zhou, H.; Pan, Z.; Liang, Z.; Zhao, C.; Zhou, Y.; Wang, F. Temperature Field Reconstruction of Concrete Dams based on Distributed Optical Fiber Monitoring Data. *Ksce. J. Civ. Eng.* **2019**, *23*, 1911–1922. [CrossRef]
27. Chen, X.; Chen, J.; Wang, T.; Zhou, H.; Liu, L. Characterization of Seepage Velocity beneath a Complex Rock Mass Dam Based on Entropy Theory. *Entropy* **2016**, *18*, 293. [CrossRef]
28. Su, H.; Hu, J.; Wen, Z. Structure analysis for concrete-faced rockfill dams based on information entropy theory and finite element method. *Int. J. Numer. Anal. Meth. Geomech.* **2011**, *36*, 1041–1055. [CrossRef]
29. Cui, H.; Jiang, S.; Ren, L.; Xiao, W.; Yuan, F.; Wang, M.; Wei, L. Dynamics and potential synchronization of regional precipitation concentration and drought-flood abrupt alternation under the influence of reservoir climate. *J. Hydrol. Reg. Stud.* **2022**, *42*, 101147. [CrossRef]
30. Lei, P.; Chang, X.; Xiao, F.; Zhang, G.; Su, H. Study on early warning index of spatial deformation for high concrete dam. *Sci. China Technol. Sci.* **2011**, *54*, 1607–1614. [CrossRef]
31. Zheng, D.; Li, X.; Yang, M.; Su, H.; Gu, C. Copula entropy and information diffusion theory-based new prediction method for high dam monitoring. *Earthq. Struct.* **2018**, *14*, 143–153. [CrossRef]
32. Huang, Y.; Wan, Z. Study on Viscoelastic Deformation Monitoring Index of an RCC Gravity Dam in an Alpine Region Using Orthogonal Test Design. *Math. Probl. Eng.* **2018**, *2018*, 8743505. [CrossRef]
33. Zhang, J.; Gu, C. Maximum Entropy Method for Operational Loads Feedback Using Concrete Dam Displacement. *Entropy* **2015**, *17*, 2958–2972. [CrossRef]
34. Qin, X.; Gu, H.; Yuan, D.; Guo, J.; Chen, X.; Xu, B.; Wu, B.; Sohn, H. An Evaluation Method of Crack Variation on Structural Performance of Concrete Dams with Fusion Entropy Based on Observation and Simulation. *Struct. Control Health Monit.* **2023**, *2023*, 4040761. [CrossRef]
35. Han, L.; Chen, M.; Sun, Z.; Si, J.; Ma, L.; Ji, W.; Zhang, H. Stability analysis of slopes based on cloud model-Monte Carlo coupling. *Front. Earth Sci.* **2023**, *11*, 1196677. [CrossRef]
36. Wu, X.; Duan, J.; Zhang, L.; AbouRizk, S.M. A hybrid information fusion approach to safety risk perception using sensor data under uncertainty. *Stoch. Environ. Res. Risk Assess.* **2017**, *32*, 105–122. [CrossRef]

37. Li, H.; Li, Z.; Ma, F.; Liu, C. Similarity analysis of dam behavior characterized by multi-monitoring points based on Cloud model. *Int. J. Distrib. Sens. Netw.* **2020**, *16*, 1550147720920226. [CrossRef]
38. Sang, L.; Wang, J.; Sui, J.; Dziedzic, M. A New Approach for Dam Safety Assessment Using the Extended Cloud Model. *Water Resour. Manag.* **2022**, *36*, 5785–5798. [CrossRef]
39. Guo, H.; Yuan, H.; Huang, Q. Structural damage identification based on gray cloud rule generator algorithm. *Adv. Mech. Eng.* **2019**, *11*, 1–13. [CrossRef]
40. Su, H.; Li, J.; Wen, Z. Evaluation of Various Temperature Control Schemes for Crack Prevention in RCC Arch Dams During Construction. *Arab. J. Sci. Eng.* **2014**, *39*, 3559–3569. [CrossRef]
41. Salazar, F.; Vicente, D.J.; Irazábal, J.; de-Pouplana, I.; San Mauro, J. A Review on Thermo-mechanical Modelling of Arch Dams During Construction and Operation: Effect of the Reference Temperature on the Stress Field. *Arch. Comput. Method. Eng.* **2020**, *27*, 1681–1707. [CrossRef]
42. Shi, N.; Chen, Y.; Li, Z. Crack Risk Evaluation of Early Age Concrete Based on the Distributed Optical Fiber Temperature Sensing. *Adv. Mater. Sci. Eng.* **2016**, *2016*, 4082926. [CrossRef]
43. An, G.; Yang, N.; Li, Q.; Hu, Y.; Yang, H. A Simplified Method for Real-Time Prediction of Temperature in Mass Concrete at Early Age. *Appl. Sci.* **2020**, *10*, 4451. [CrossRef]
44. Li, M.; Si, W.; Du, S.; Zhang, M.; Ren, Q.; Shen, Y. Thermal deformation coordination analysis of CC-RCC combined dam structure during construction and operation periods. *Eng. Struct.* **2020**, *213*, 110587. [CrossRef]
45. de Oliveira, J.R.S.; Pettres, R. A thermal analysis of concrete structures performed by layers using boundary element formulation and dual reciprocity. *Eng. Anal. Bound. Elem.* **2023**, *150*, 542–554. [CrossRef]
46. Wang, L.; Yang, H.; Zhou, S.; Chen, E.; Tang, S. Mechanical properties, long-term hydration heat, shinkage behavior and crack resistance of dam concrete designed with low heat Portland (LHP) cement and fly ash. *Constr. Build. Mater.* **2018**, *187*, 1073–1091. [CrossRef]
47. Cho, H.; Lee, E.-K. Tree-Structured Regression Model Using a Projection Pursuit Approach. *Appl. Sci.* **2021**, *11*, 9885. [CrossRef]
48. Lee, E.-K. PPtreeViz: An R Package for Visualizing Projection Pursuit Classification Trees. *J. Stat. Softw.* **2018**, *83*, 1–30. [CrossRef]
49. Cao, C.; Song, S.; Chen, J.; Zheng, L.; Kong, Y. An Approach to Predict Debris Flow Average Velocity. *Water* **2017**, *9*, 205. [CrossRef]
50. An, H.; Yang, W.; Huang, J.; Huang, A.; Wan, Z.; An, M. Identify and Assess Hydropower Project's Multidimensional Social Impacts with Rough Set and Projection Pursuit Model. *Complexity* **2020**, *2020*, 9394639. [CrossRef]
51. Jin, Y.; Sun, Y.; Ma, H. A Developed Artificial Bee Colony Algorithm Based on Cloud Model. *Mathematics* **2018**, *6*, 61. [CrossRef]
52. Gao, H.; Zhang, X.; Liu, Y.; Li, D. Cloud Model Approach for Lateral Control of Intelligent Vehicle Systems. *Sci. Program.* **2016**, *2016*, 6842891. [CrossRef]
53. Jiao, S.; Pan, Z.; Chen, Y.; Li, Y. Cloud Annealing: A Novel Simulated Annealing Algorithm Based on Cloud Model. *IEICE Trans. Inf. Syst.* **2020**, *E103-D*, 85–92. [CrossRef]
54. Khatri, P.; Hayasaka, T.; Holben, B.N.; Singh, R.P.; Letu, H.; Tripathi, S.N. Increased aerosols can reverse Twomey effect in water clouds through radiative pathway. *Sci. Rep.* **2022**, *12*, 20666. [CrossRef]
55. Zhu, F. Mathematical Modeling Method of the Improved Genetic Algorithm for Random Power Fluctuation. *Int. T. Electr. Energy Syst.* **2022**, *2022*, 1889952. [CrossRef]
56. Liu, Y.; Chen, X.; Wang, H. The fused Kolmogorov–Smirnov screening for ultra-high dimensional semi-competing risks data. *Appl. Math. Model.* **2021**, *98*, 109–120. [CrossRef]
57. Lee, S.-H.; Lee, J.-W.; Kim, M.-K.; Park, H.-M. An Analysis on the Effectiveness of Nitrogen Oxide Reduction from Applying Titanium Dioxide on Urban Roads Using a Statistical Method. *Atmosphere* **2021**, *12*, 972. [CrossRef]


**Disclaimer/Publisher's Note:** The statements, opinions and data contained in all publications are solely those of the individual author(s) and contributor(s) and not of MDPI and/or the editor(s). MDPI and/or the editor(s) disclaim responsibility for any injury to people or property resulting from any ideas, methods, instructions or products referred to in the content.